B1210

Combined effects of A-site non-stoichiometry, crystal structure, and microstructure for the enhanced catalytic activity of (LaSr)(CoFe)$O_{3-\delta}$ cathodes for IT-SOFCs

Ozden Celikbilek (1,2), Cam-Anh Thieu (3,4), Fabio Agnese (5), Eleonora Cali (2), Christian Lenser (6), Norbert H. Menzler (6), Ji-Won Son (3,4), Stephen J. Skinner (2), Elisabeth Djurado (1)

(1) Univ. Grenoble Alpes, Univ. Savoie Mont Blanc, CNRS, Grenoble INP, LEPMI, 38000, Grenoble/France

(2) Department of Materials, Imperial College London Prince Consort Road, SW7 2BP, London/United Kingdom

(3) Center for Energy Materials Research, Korea Institute of Science and Technology (KIST), Hawolgok-dong, Seongbuk-gu, 02792 Seoul/Korea

(4) Division of Nano & Information Technology, KIST School, Korea University of Science and Technology (UST), Hawolgok-dong, Seongbuk-gu, 02792 Seoul/Korea

(5) Univ. Grenoble Alpes, INAC-SyMMES, F-38054 Grenoble Cedex 9/France

(6) Forschungszentrum Jülich GmbH, Institute of Energy and Climate Research: Materials Synthesis and Processing (IEK-1), 52425 Jülich/Germany

Tel: +447378171611

o.celikbilek@imperial.ac.uk

Abstract

The high oxygen reduction reaction (ORR) activity of the A-site deficient $(La_{0.7}Sr_{0.3})_{0.95}(Co_{0.2}Fe_{0.8})O_{3-\delta}$ (LSCF) film makes it an excellent cathode material for intermediate temperature solid oxide fuel cell (IT-SOFC) applications. The cathode was deposited by the electrostatic spray deposition (ESD) technique which provided microstructural details at the nanometre length scale (~100 nm).[1] The area-specific resistance values as low as 0.037 and 0.1 Ω cm^2 were measured in a symmetrical cell and power density of 0.87 and 0.50 W cm^{-2} at 0.7 V in a Ni/YSZ anode-supported cell at 650 and 600 °C, respectively were obtained. The A-site deficiency resulted in the precipitation of a B-site spinel phase composed of $CoFeO_x$ (CFO), while the perovskite structure of LSCF was modified to closely related two-phase perovskite structures. Detailed microstructural analyses showed that well-dispersed, nanoscale (~10-20 nm) CFO phase decorated the LSCF surfaces. Such substantial increase in the ORR kinetics was attributed to the catalytically active and nanostructured CFO precipitates and the very high active surface area of the ESD film.

[1] O. Celikbilek, C.-A. Thieu, F. Agnese, E. Cali, C. Lenser, N. H. Menzler, J.-W. Son, S. J. Skinner and E. Djurado, *J. Mater. Chem. A*, 2019, **7**, 25102–25111.

1. Introduction

The low-temperature operation provides great benefits for the deployment of solid oxide cells (SOCs) in the mobile/transport applications.[2,3] However, the reaction kinetics of existing materials become sluggish at low temperatures. Microstructure and materials design were shown effective to improve the electrodes' performance up to an order of magnitude.[4]

In terms of materials design, combinations of slight A- or B-site excess/deficiency have been explored in the ABO_3-type family of perovskites. Particularly, it was shown that A-site deficiency created additional oxygen vacancies to improve the ionic conductivity and the stability of a phase.[5] In terms of composition, $(LaSr)(CoFe)O_{3-\delta}$ (LSCF) is among the most studied ABO_3-type perovskites and still attracts a lot of interest. However, a very narrow stability regime was shown for these types of materials.[6] Slight deviations from A-site to B-site ratio result in the formation of a Ruddlesden-Popper type layered perovskite in the case of A-site excess and a spinel oxide in the case of B-site excess. It is, however, unclear how the catalytic activity is affected by the secondary phase formations as a result of the changes in the stoichiometry.

In this work, $(La_{0.7}Sr_{0.3})_{0.95}(Co_{0.2}Fe_{0.8})O_{3-\delta}$ (referred to as A-site deficient LSCF) composition was investigated by structural, microstructural, and electrochemical characterization techniques. The films were deposited by the electrostatic spray deposition (ESD) technique which provided microstructural features at the nanometre length scale.[7] Scanning electron microscopy (SEM), powder X-ray diffraction (XRD), scanning transmission electron microscopy (STEM) coupled with energy-dispersive X-ray spectroscopy (EDX), and electrochemical impedance spectroscopy (EIS) were employed to study the catalytic effect of A-site deficiency on the electrode performance.

2. Experiments

The cathode layer included a double layer architecture consisting of LSCF layer deposited by the ESD and topped by a screen-printed current collecting layer (CCL). ESD films were deposited using a vertical setup starting from precursor salt solutions. Appropriate amounts of $La(NO_3)_3.6H_2O$ (Prolabo, 99.99%), $SrCl_2.6H_2O$ (Strem Chemicals, 99%), $Co(NO_3)_2.6H_2O$ (Sigma-Aldrich, 99.999%) and $Fe(NO_3)_2.9H_2O$ (Sigma-Aldrich, 99.99%) salts were dissolved in absolute ethanol (99.9%; Prolabo) and butyl carbitol (99+%; Acros Organics) with a 1:2 volume ratio and a total salt concentration of 0.02 mol L^{-1}. The solution was sprayed onto the substrate. ESD deposition parameters comprise a substrate temperature of 300 °C, a nozzle to substrate distance of 15 mm, the voltage of ~5-6 kV, and a flow rate of 1.5 mL h^{-1}. Crystallization of the films and sintering were achieved at 900 °C for 2 h at a 2 °C min^{-1} heating rate and a 3 °C min^{-1} cooling rate. The targeted stoichiometry of the LSCF was $La_{0.6}Sr_{0.4}Co_{0.2}Fe_{0.8}O_{3-\delta}$ (LSCF 6428). However, analysis by inductively coupled plasma-optical emission spectrometry (ICP-OES) (iCAP 6500 Thermo Scientific, USA) showed the average stoichiometry of the film to be $(La_{0.71}Sr_{0.29})_{0.95}Co_{0.17}Fe_{0.83}O_{3-\delta}$. In the text, it was simplified to $(La_{0.7}Sr_{0.3})_{0.95}Co_{0.2}Fe_{0.8}O_{3-\delta}$ and will be referred to as A-site deficient LSCF.

Scanning electron microscopy (SEM) was used to study the microstructure of the films, using a field emission gun (ZEISS Ultra 55) operating at an accelerating voltage of 3 kV and an average of 7 mm working distance. The HR-TEM analysis was carried out on a

JEOL 2100F microscope equipped with an Oxford Instruments EDX detector. EDX was performed in STEM mode with an annular dark field detector.

Impedance spectroscopy was used to evaluate the electrochemical response. Symmetrical cell measurements in open-circuit voltage (OCV) mode were carried out in ambient air with between 450 and 650 °C. An Autolab frequency response analyzer operating between 10 kHz and 0.05 Hz was used. The amplitude of the measuring signal was adjusted to 20 mV. The data were fitted with electrical equivalent circuits using the EC-Lab® software (V10.44).

Single-cell tests were performed on anode-supported cells prepared at Forschungszentrum Jülich, Germany. The cells were based on tape-cast NiO-YSZ supports of ~300 µm thickness, and screen-printed NiO-YSZ anodes were obtained from CeramTec GmbH (Marktredwitz, Germany). The 1.5 µm thin YSZ electrolyte was prepared by the sequential deposition of YSZ nano-dispersion and polymeric sol, followed by co-sintering of the half-cell at 1400 °C.[8] Subsequently, a ~ 0.5 µm thin $Gd_{0.2}Ce_{0.8}O_{1.9}$ diffusion barrier layer was deposited via Magnetron Sputtering. The LSCF cathode prepared via ESD had 10 x 10 mm² dimension. A-site deficient $La_{0.58}Sr_{0.4}Co_{0.2}Fe_{0.8}O_{3-\delta}$ ink (FZ-Jülich, Germany) was screen printed on the LSCF films deposited by the ESD to serve as CCL and sintered at 850 °C for 2 h in air. Measurements were performed in the temperature range of 450-650 °C, using an Iviumstat test apparatus in a frequency range between 1 MHz and 0.1 Hz. Air on the cathode side and humidified H_2 on the anode side with a fuel composition of 97 vol. % H_2 and 3 vol. % H_2O at a flow rate of 200 standard cm^3 min^{-1} (sccm) was used. A modified interconnect rib design with gold mesh with openings of 250 µm by 250 µm was used for the cell test. Current vs voltage data were recorded between 650 °C and 450 °C at each 50 °C in descending order. A Solartron impedance analyser with an electrochemical interface (SI 1260) and an Iviumstat electrochemical analyser (Iviumstat, Ivium Technologies) was used to obtain these EIS and I-V-P curves. The AC amplitude of the impedance measurements was set to 50 mV.

3. Results

ESD is a unique technique to obtain micrometre-thick films with nanometric features. SEM micrographs in Figure 1 demonstrate the micro- and nanostructure of ~10 µm-thick cathode films made up of large columnar-like blocks separated by ~1-2 µm wide interconnected gas diffusion channels. The grain and porosity sizes within the columnar blocks show a scale of ~100 nm. The cross-sectional view (Figure 1d) provides an overview of the nanometre length scale features of the LSCF ESD films compared with screen printed CCL of the same material. In a previous work, the porosity, specific surface area and tortuosity values of LSCF ESD films were calculated as 22 ± 7 %, 19 ± 6 μm^{-1}, and 1.50 ± 0.2, respectively.[7]

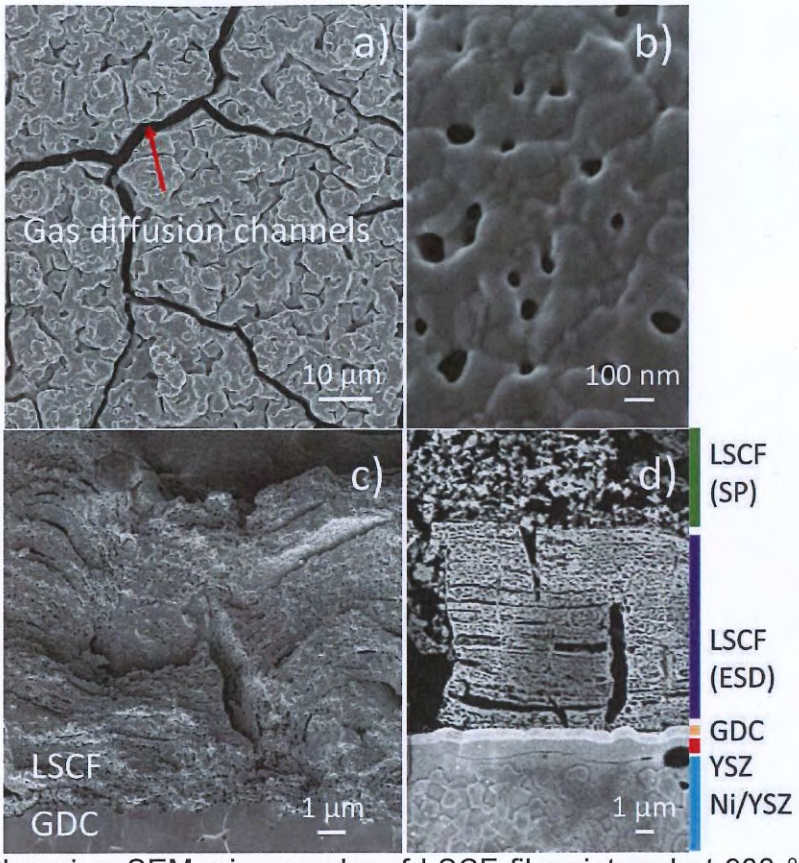

Figure 1. a-b) Plan view SEM micrographs of LSCF film sintered at 900 °C for 2 h in air, Cross-sectional SEM micrograph of c) LSCF film on GDC electrolyte and d) As-deposited LSCF film on anode-supported bi-layer electrolyte cell. The colored bars next to d) show each layer in the cell. Reproduced from Ref. [1] with permission from The Royal Society of Chemistry.

Figure 2a shows the XRD pattern and the structural refinement of the ESD cathode layer on the GDC electrolyte. Notably, three phases can be observed; the LSCF phase (ICDD: 04-020-8368) with *R*■ space group (No. 167), the GDC phase (ICDD: 04-012-3418) with *Fm*■*m* space group (No. 225), and a third phase corresponding well to a spinel crystal structure (*Fd*■*m*) with a unit cell parameter of 8.3204(7) Å. The amount of this phase with respect to the LSCF was found to be ~6 wt. %. As can be seen in the inset of Figure 2a, the refinement of the LSCF with one rhombohedral phase did not yield a good fitting. Instead, two rhombohedral phases with slightly different *a, b* and *c* parameters gave an improved fit (Figure 2b). Similar behaviour was observed in previous reports on A-site non-stoichiometric LSCF.[9] The first phase was fitted with *a, b* = 5.48(8) Å and *c* = 13.50(2) Å and the second phase was fitted with *a, b* = 5.47(9) Å and *c* = 13.56(4) Å.

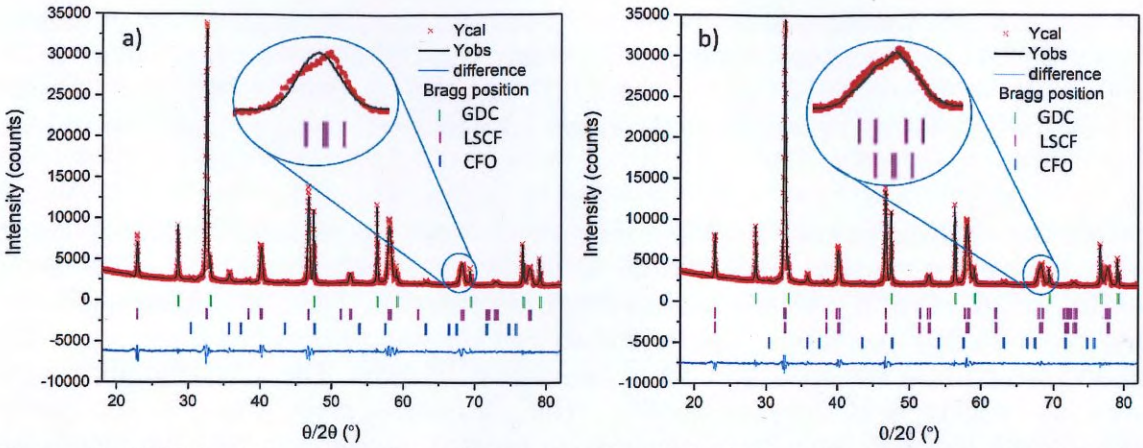

Figure 2. XRD lattice parameter refinement of an LSCF film deposited on GDC electrolyte sintered at 900 °C for 2 h in air. a) one rhombohedral phase and b) two rhombohedral phases. Reproduced from Ref. [1] with permission from The Royal Society of Chemistry.

Next, STEM-EDX was used to investigate the elemental composition of the minority third phase. The STEM-EDX maps in Figure 3 demonstrate the presence of only La, Sr, Co, Fe, and O elements with some particles containing solely Co and Fe and O. These particles are smaller than a typical LSCF grain, with an average grain size of ~20 nm.

Elemental point analysis at three different locations shows that the particle containing Co and Fe elements had a Co: Fe ratio of approximately 1.0. In the literature, common cobalt ferrite spinel structures were reported as $CoFe_2O_4$ (ICDD: 04-006-4147) and Co_2FeO_4 (ICDD: 04-016-3952). In the rest of the text, $CoFeO_x$ will be referred to as CFO. Point analyses from the other two locations gave La: Sr ratio of ~3.7. It is important to note that, this value is higher than the value obtain from ICP-OES analysis (~2.4). The discrepancy can be due to the amount of investigated particles. While ICP-OES provides average information from the ensemble of all particles, EDX gives point analysis on a few selected particles. Nevertheless, both techniques gave A: B site ratio as ~0.95:1.00. As mentioned above, the targeted stoichiometry for the cathode film was LSCF 6428. The origins of the A-site deficiency is not known at the moment, but it might be related to the precursor purity and/or solubility limits of the metal-nitrates as well as the non-equilibrium state of the ESD technique.

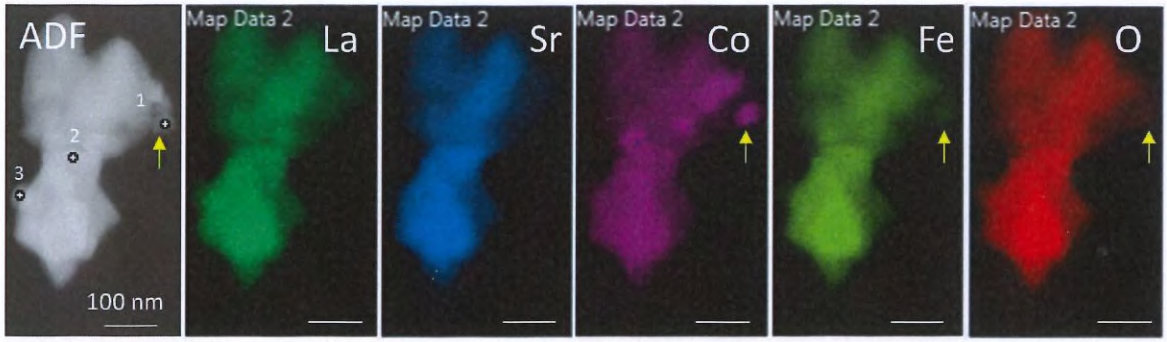

Figure 3. STEM ADF-EDX elemental maps of the particles removed from the film. The intensity of the maps represents the net EDX counts after corrections for background and peak overlap. Reproduced from Ref. [1] with permission from The Royal Society of Chemistry.

Figure 4 shows the Arrhenius plot of area-specific polarization resistance (ASR) of various LSCF films on GDC electrolytes measured between 450-650 °C in air and under OCV. The plot shows ASR values of as low as 0.037 and 0.1 Ω cm^2 at 650 and 600 °C, respectively for LSCF (ESD). Moreover, it shows an activation energy (E_a) value of ~1.5 eV.

To separate the catalytic activity of CFO nanoparticles from the structural changes due to A-site non-stoichiometry, new experiments were designed. Stoichiometric LSCF 6428 (Sigma-Aldrich, 10-14 m^2 g^{-1}) were measured as bare samples. Then, a CFO solution was infiltrated into the LSCF backbone. The infiltration method was selected as it can mimic the amount and the particle sizes of CFO, as obtained in ESD films. The infiltrated films were measured on-heating and then on-cooling. The Arrhenius plots show a substantial decrease in both the ASR and the E_a values on heating, suggesting that the increased catalytic activity is in fact due to CFO nanoparticles. It can be seen that during cooling, both values increased. Notably, the E_a value increased from ~1.0 (on heating) to ~1.5 eV (on cooling) and became similar to LSCF (ESD) films. This is attributed to the agglomeration of CFO nanoparticles, similar to those reported for Co_3O_4 at elevated temperatures.[10]

These experiments suggest that CFO nanoparticles indeed improve the catalytic activity when decorated on LSCF films. We would like to point out the importance of micro- and nanostructure optimisation of cathode layers. Architectural engineering of ESD films topped with CCL can decrease the ASR values up to an order of magnitude.

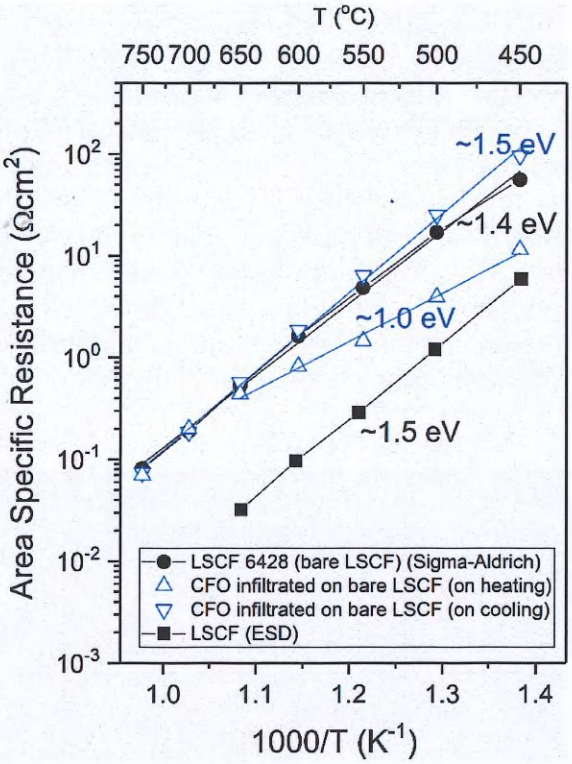

Figure 4 Arrhenius plot of ASR of total polarization losses of symmetrical LSCF 6428 bare (commercial powder), CFO infiltrated LSCF 6428, and LSCF (ESD). Reproduced from Ref. [1] with permission from The Royal Society of Chemistry.

Figure 5 shows the current-voltage-power (I – V – P) curves and the corresponding Nyquist plots measured at 0.75 V. The current density at a cell voltage of 0.7 V was 1.2 and 0.7 A cm^{-2} at 650 and 600 °C, respectively. The peak power density at 600 °C in this work is among the highest values for LSCF-based cathodes.[11,12] Unlike this work, the electrodes in references [11,12] contain an LSCF/GDC layer either as a barrier layer or as a current-conducting layer. On the other hand, similar to our columnar-like LSCF cathode microstructure, Hsu *et al.* also used the ESD technique to deposit an LSCF cathode on Ni-SDC based anode-supported cells.[13] They reported a 0.9 W cm^{-2} peak power density at 600 °C with a significantly lower current density at 0.7 V in comparison to this work.

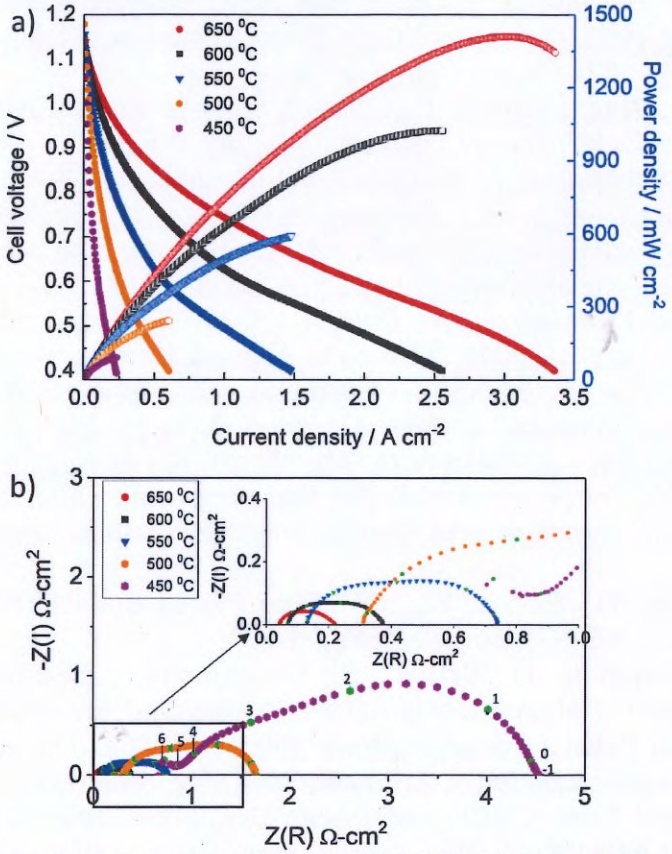

Figure 5. **I-V-P curves and corresponding Nyquist impedance plots of LSCF/GDC/YSZ/Ni-YSZ cells measured at 0.75 V with 3 % humidified hydrogen in the anode side.** The green points are frequency values on a logarithmic scale. Reproduced from Ref. [1] with permission from The Royal Society of Chemistry.

4. Conclusions

A-site deficient $(La_{0.7}Sr_{0.3})_{0.95}Co_{0.2}Fe_{0.8}O_{3-\delta}$ (LSCF) films prepared by the ESD technique were investigated as air electrodes for high-performance SOCs. A-site deficiency caused the precipitation of B-site elements and also led to the separation of single-phase rhombohedral LSCF into two closely related rhombohedral phases. The precipitated nanoparticles of B-site elements ~$CoFeO_x$ (CFO) had an average particle size of ~20 nm and they homogeneously decorated the LSCF surfaces. The films gave very low ASR values of 0.037, 0.100 Ω cm^2 on symmetrical cells, and power densities of 1.2 and 0.7 A cm^{-2} at 0.7 V on a Ni/YSZ anode-supported cell at 650 and 600 °C, respectively. The catalytic effect of CFO nanoparticles was investigated on an additional set of controlled experiments. CFO solution was infiltrated on the stoichiometric LSCF phase to separate

the A-site non-stoichiometry effects from the catalytic activity of CFO nanoparticles. A decrease in both the activation energy and ASR values was observed. These findings demonstrate that high performance is partly due to the nanostructured B-site precipitates decorating the LSCF surfaces and partly to the unique microstructural details in the ESD films.

References

[1] Celikbilek, O.; Thieu, C.-A.; Agnese, F.; Calì, E.; Lenser, C.; Menzler, N. H.; Son, J.-W.; Skinner, S. J.; Djurado, E., 2019 "Enhanced catalytic activity of nanostructured, A-site deficient (La0.7Sr0.3)0.95(Co0.2Fe0.8)O3-δ for SOFC cathodes" J Mater Chem A, **7**, pp 25102–11.

[2] Hussain, A. M.; Wachsman, E. D., 2019 "Liquids-to-Power Using Low-Temperature Solid Oxide Fuel Cells" Energy Technol., **7** (1), pp. 20–32.

[3] Udosmilp, D.;Rechberger, J.; Neubauer, R.; Bischof, C.; Thaler, F.; Schafbauer, W.; Menzler, N.H.; de Haart, L.G.J.; Nenning, A.; Opitz, A.K.; Guillon, O.; Bram, M., 2020 "Metal-supported solid oxide fuel cells with excetionally high power density for range extender systems" Cell Reports Phys. Sci. **1,** pp. 100072

[4] Ma, W.; Kim, J. J.; Tsvetkov, N.; Daio, T.; Kuru, Y.; Cai, Z.; Chen, Y.; Sasaki, K.; Tuller, H. L.; Yildiz, B., 2015 "Vertically Aligned Nanocomposite La0.8Sr0.2CoO3 /(La0.5Sr0.5)2CoO4 Cathodes – Electronic Structure, Surface Chemistry and Oxygen Reduction Kinetics" J. Mater. Chem. A, **3** (1), pp. 207–219.

[5] Mineshige, A.; Izutsu, J.; Nakamura, M.; Nigaki, K.; Abe, J.; Kobune, M.; Fujii, S.; Yazawa, T., 2005 "ntroduction of A-Site Deficiency into La0.6Sr0.4Co0.2Fe0.8O3–δ and Its Effect on Structure and Conductivity" Solid State Ionics, **176** (11–12), pp. 1145–1149.

[6] Morin, F.; Trudel, G.; Denos, Y., 1997 "The Phase Stability of La0.5Sr0.5CoO3-δ" Solid State Ionics, **96** (97), pp.129–139.

[7] Celikbilek, O.; Jauffrès, D.; Siebert, E.; Dessemond, L.; Burriel, M.; Martin, C. L.; Djurado, E., 2016 "Rational Design of Hierarchically Nanostructured Electrodes for Solid Oxide Fuel Cells" J Power Sources, **333**, pp. 72–82.

[8] Menzler, N. H.; Malzbender, J.; Schoderböck, P.; Kauert, R.; Buchkremer, H. P., 2014 "Sequential Tape Casting of Anode-Supported Solid Oxide Fuel Cell" Fuel Cells, **14** (1), pp. 96–106.

[9] Hansen, K. K.; Vels Hansen, K., 2007 "A-Site Deficient (La0.6Sr0.4)1-SFe0.8Co0.2O3-δ Perovskites as SOFC Cathodes" Solid State Ionics, **178** (23–24), pp. 1379–1384.

[10] Ren, Y.; Cheng, Y.; Gorte, R. J.; Huang, K., 2017 "Toward Stabilizing Co3O4 Nanoparticles as an Oxygen Reduction Reaction Catalyst for Intermediate-Temperature SOFCs" J. Electrochem. Soc., **164** (10), pp. F3001–F3007.

[11] Oh, E. O.; Whang, C. M.; Lee, Y. R.; Park, S. Y.; Prasad, D. H.; Yoon, K. J.; Son, J. W.; Lee, J. H.; Lee, H. W., 2012 "Extremely Thin Bilayer Electrolyte for Solid Oxide Fuel Cells (SOFCs) Fabricated by Chemical Solution Deposition (CSD)" Adv. Mater., **24** (25), pp. 3373–3377.

[12] Jang, I.; Kim, S.; Kim, C.; Yoon, H.; Song, T., 2018 "Enhancement of Oxygen Reduction Reaction through Coating a Nano-Web-Structured La0.6Sr0.4Co0.2Fe0.8O3-δ Thin-Film as a Cathode/Electrolyte Interfacial Layer for Lowering the Operating Temperature of Solid Oxide Fuel Cells" J. Power Sources, **392**, pp. 123–128.

[13] Hsu, C.-S. S.; Hwang, B.-H. H.; Xie, Y.; Zhang, X, 2008 "Enhancement of Solid Oxide Fuel Cell Performance by La0.6Sr0.4Co0.2Fe0.8O3−δ Double-Layer Cathode" J. Electrochem Soc., **155** (12), pp. B1240–B1243.